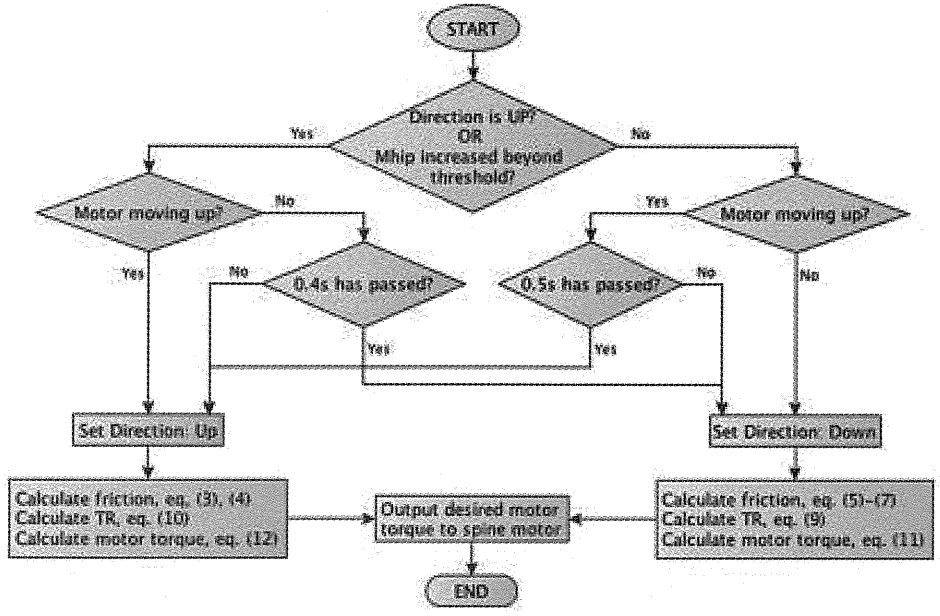

Figure 11 : Block diagram of the direction decision algorithm that chooses between the down and up state. Time constants were determined experimentally.

3. EXPERIMENT and RESULTS

Experiments with have been performed with the exo-spine to verify its flexibility and assisting ability by measuring its full ROM and by a subject performing representative lifting actions. To exclude other influences and focus on the performance of the exo-spine only there were no other active DOF. Simplified arms with each a passive free joint for inner arm rotation and lockable shoulder (flexion) joints and elbow joints, as well as simplified legs with a locked hip joint were attached (Fig. 6).

3.1. Range of motion measurement

As a test of basic flexibility the full ROM of both the top of the exo-spine and a point on its left shoulder, directly behind and next to the wearer's shoulder, have been measured using motion capture. The inner arm rotation joints were locked, as these are not the focus of this research.

The results are shown in Fig. 12. This ROM was measured without a wearer and thus does not take into account any space constraints such as exoskeleton design or wearer body size. Single-DOF motion is indicated with the red areas in Fig. 12 ((a) flexion, (b) lateral flexion, (c) rotation). The maximum range for each single DOF is 44deg flexion (0.77rad, equal to α_{A1} = 0.95 rad), 33deg (0.58rad) lateral flexion, 32deg (0.56rad) rotation and 64 mm of forward abduction at the endpoints of the shoulder blades. The blue areas show the reachable space when using all DOF.

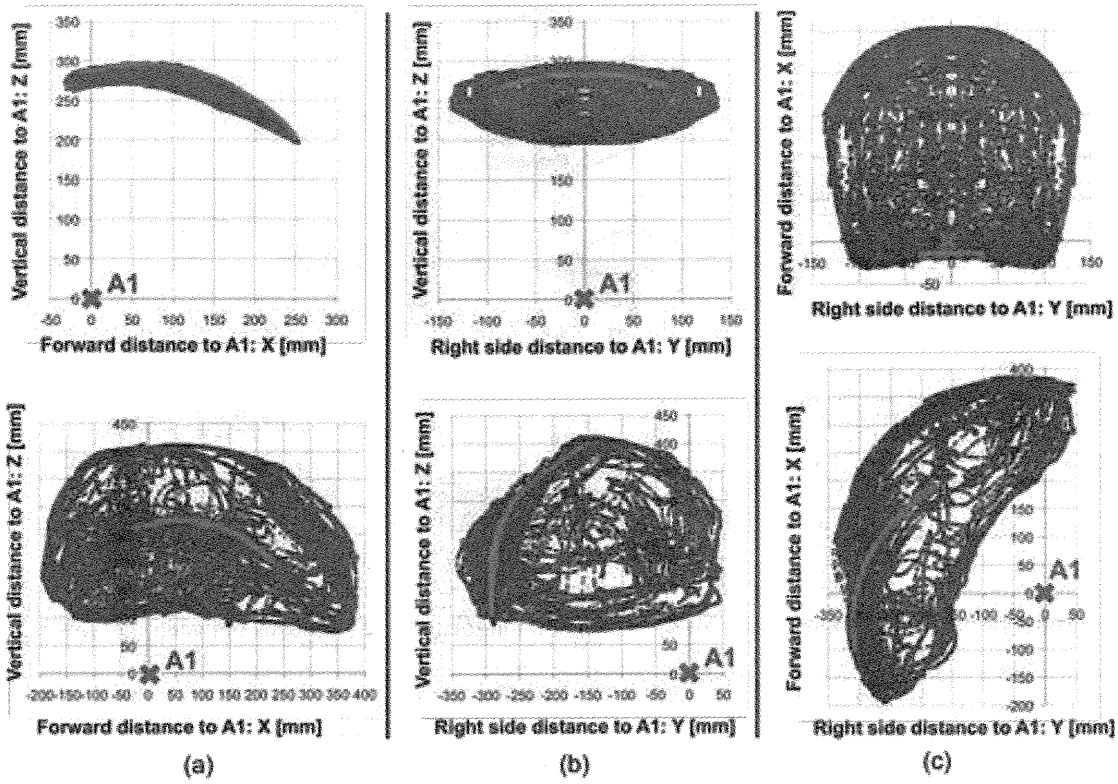

Figure 12 : ROM as measured by motion capture, and without wearer, shown in (a) right side view, (b) rear view, and (c) top view for a point at the front of the top vertebra (top row) and for a point at the rear of the left shoulder (bottom row, note the difference in scale). Based on symmetry the data for the top vertebra was mirrored over the XZ (sagittal) plane. Red, inner areas indicate the ROM during (a) flexion, (b) lateral flexion, and (c) rotation.

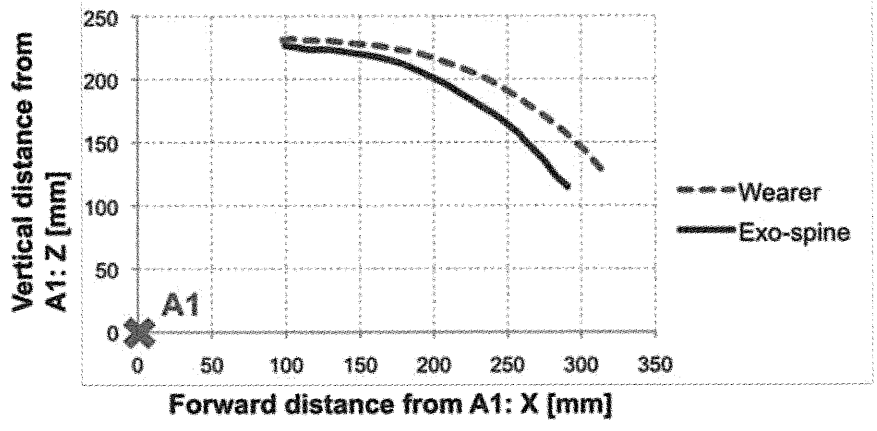

Figure 13 : Side view of the paths of both the exo-spine's and wearer's glenohumeral joints when flexing forward.

The exo-spine is designed to extend when bending, but with the ICOR moving backward during flexion the extension becomes slower (per unit flexion), and, as shown in Fig. 13, some mismatch

between the both exo-spine's and the wearers shoulder remains at higher flexion angles. This is, however, not bad as long as the upper arm cuff is positioned close to the elbow and allows at least some rotation; although an additional passive translation DOF that allows the arm cuffs to slide up would also be preferred [10].

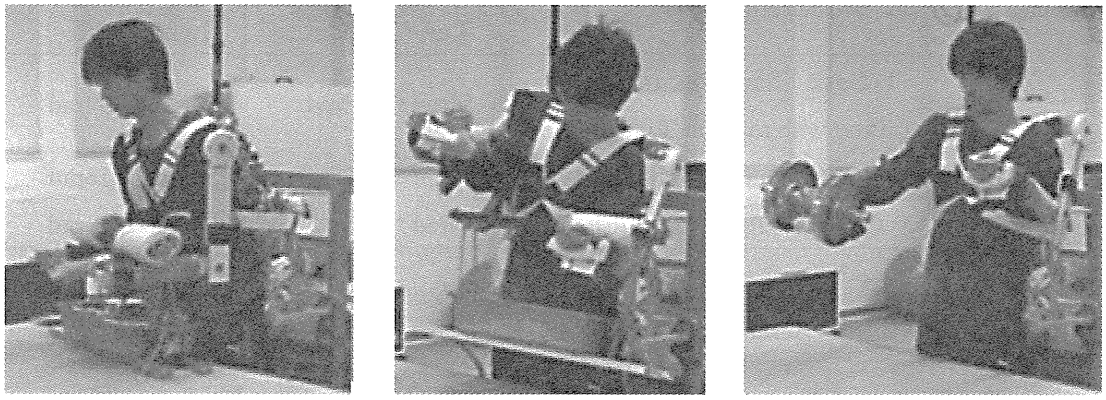

Figure 14 : Experiment snapshots for (a) lifting with rotation, (basic lifting is similar but without spinal rotation), (b) lifting with lateral flexion, (c) one arm lifting.

3.2. Lifting experiments and results

Four different lifting experiments have been performed to confirm the performance of the exo-spine. While all four are, mechanically, fundamental movements, they are also based on specific nursing actions [2] [20] [21]. Although spine motion is advised against for nursing tasks, it could become allowed when an exoskeleton provides most of the support. The experiments are:

1 Basic lifting

Lifting up and setting down using only spine flexion, using loads of 20, 30, and 40 kg placed on the lower arms. Particularly used in patient transfer tasks, although the position of the load may be different there.

2 Lifting with rotation

Lifting up, rotating with load from left to right (or vice-versa) as far as possible, setting down, using loads of 20, 30, and 40 kg. Used in patient repositioning tasks.

3 Lifting with lateral flexion

The load in the experiment was asymmetric, such that one arm has to be higher to hold the load horizontal (Fig. 14b). Actions were: lifting up, going down while bringing load horizontal, setting down, with loads of 20, 30, and 40 kg. Used when one arm is at a higher position than the other, such as when lifting up someone's legs onto the bed.

4 One arm lifting

Lifting up with one stretched arm (most extreme reaching case), and setting down, using loads

of 10 and 15 kg (additional wrist support was provided). Used when reaching over the bed to lift up or pull a part of the patient.

Table 1: Shoulder and elbow angles during experiments.

Experiment	Shoulder angle Left / Right	Elbow angle Left / Right
1) Basic lifting, Fig. 14a 2) Lifting with rotation, Fig. 14a	0.54rad / 0.54rad	1.54rad / 1.54rad
3) Lifting with lateral flexion, Fig. 14b	0.54rad / 1.08rad	1.54rad / 1.16rad
4) One arm lifting, Fig. 14c	0.54rad / 1.35rad	1.54rad / 0.13rad

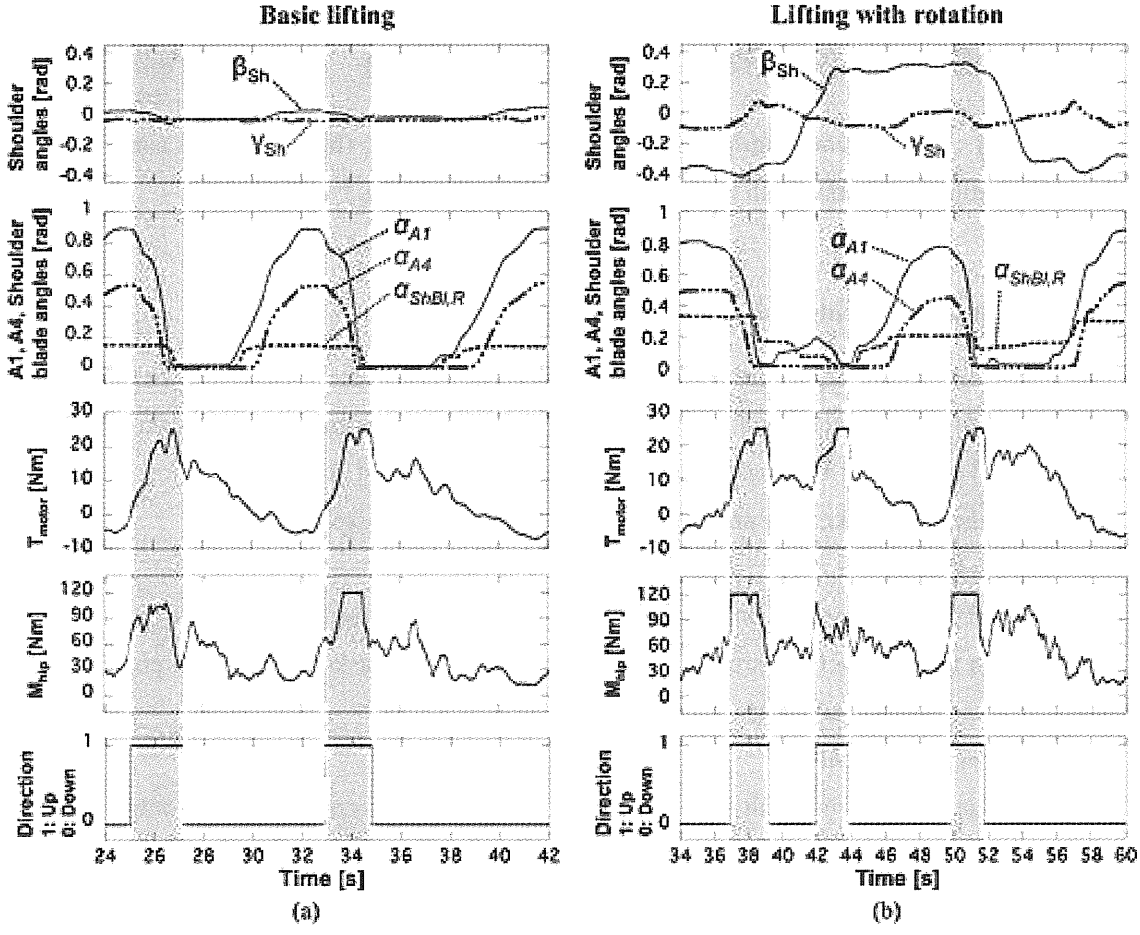

Figure 15 : Experiment results showing two lifting cycles for (a) experiment 1 (basic lifting, 20 kg), and (b) experiment 2 (lifting with rotation, 30 kg). Shown are, from the top, the angles of the exo-spine's shoulder girdle: rotation β_{Sh} and lateral flexion γ_{Sh}, the exo-spine's joint angles A1 (α_{A1}), A4 (α_{A4}) and right shoulder blade ($\alpha_{ShBl,R}$), motor torque T_{motor}, hip moment, M_{hip}, commanded by the wearer's BES, and the controller's direction status, with 1 indicating up (grey areas).

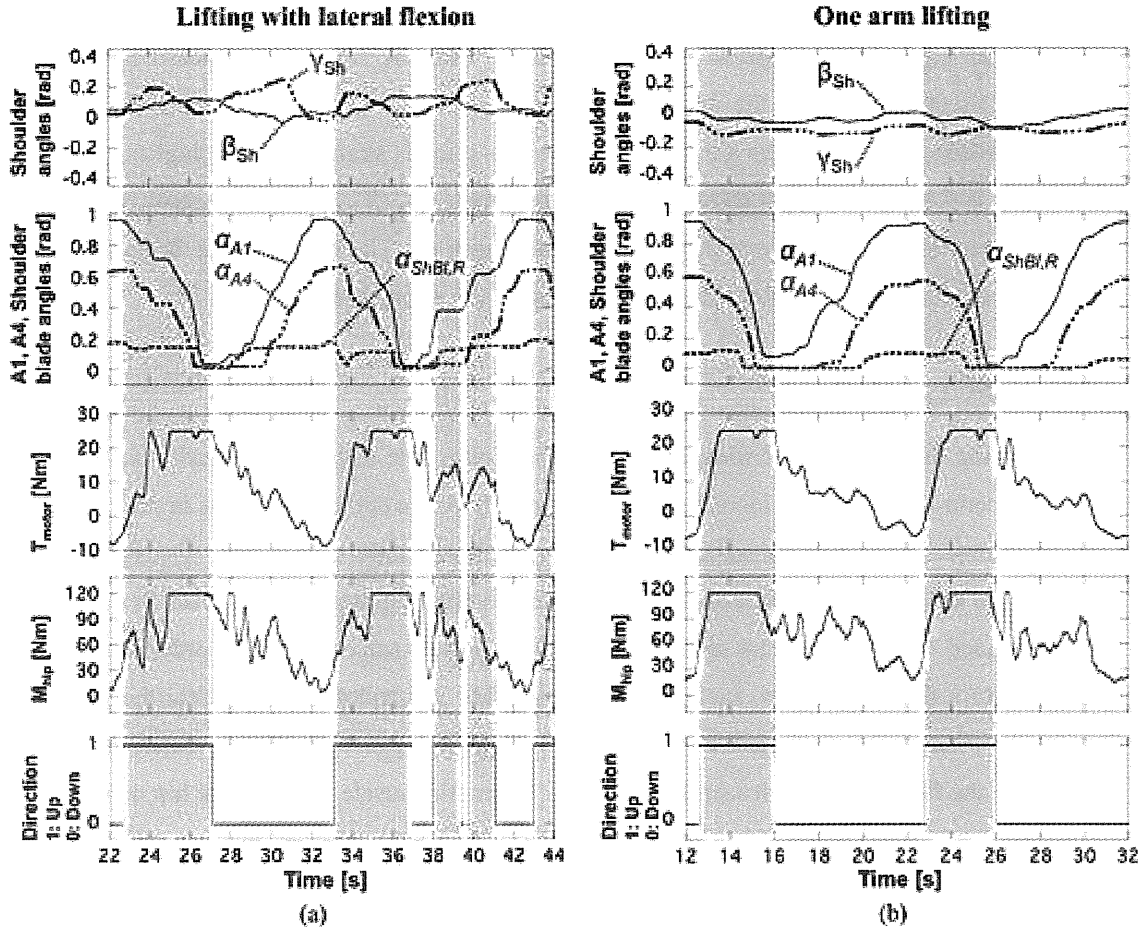

Figure 16 : Experiment results showing two lifting cycles for (a) experiment 3 (lifting with lateral flexion, 40 kg), and (b) experiment 4 (one arm lifting, 15 kg). Shown are, from the top, the angles of the exo-spine's shoulder girdle: rotation β_{Sh} and lateral flexion γ_{Sh}, the exo-spine's joint angles A1 (α_{A1}), A4 (α_{A4}) and right shoulder blade ($\alpha_{ShBl,R}$), motor torque T_{motor}, hip moment, M_{hip}, commanded by the wearer's BES, and the controller's direction status, with 1 indicating up (grey areas).

The angles of the shoulders and elbows during the experiments are listed in Table 1. There were several safety precautions including torque limitations (maximum T_{motor}: 25 Nm, maximum M_{hip}: 120 Nm), a dead-man switch, and the placement of the loads below the wearer's arms using a beam with ropes, as in Fig. 14a and b. The subject was an adult male (1.72m, 52 kg) with prior operating experience of other HAL robot suits. He was fixed to the system using straps at the legs and arms and bands that cross the chest, similar to general full body exoskeletons. To measure M_{hip}, which is always an extension torque during lifting, the BES of each leg's hip extensor, gluteus maximus, was measured.

Figures 15 and 16 show typical examples of experiment results for two lifting cycles each of 20 kg basic lifting (15a), 30 kg lifting with rotation (15b), 40 kg lifting with lateral flexion (16a), and 15 kg one arm lifting (16b). At the top are shown the angles of the line connecting the glenohumeral joints

of the exo-spine, with β_{Sh} indicating rotation (as viewed from above, projected onto the horizontal XY plane), and γ_{Sh} indicating lateral flexion (the angle with the XY plane), measured using motion capture. Directly below are the angles of the exo-spine's joint A1 (α_{A1}), joint A4 (α_{A4}) and right shoulder blade ($\alpha_{ShBl,R}$). Angles are zero when the exo-spine is straight up. The highest possible value for $\alpha_{ShBl,R}$ is 0.47rad at 64 mm abduction. Next are shown M_{hip}, T_{motor}, and the motor controller's state for the direction, up or down, with grey areas indicating up. The motor torque becomes negative at times to compensate for the motor friction and, partly, the spring pre-tension.

4. DISCUSSION

In the lifting experiment described above the subject was able to lift up all loads successfully. Each time the controller noted the increase in muscle activity of the subject, and thus in M_{hip}, and switched to the up state, after which the subject could lift up the load within 1s to 4s time. Occasionally, such as in Fig. 15b at 42s, it was necessary to extend the exo-spine up again after it had flexed down more than intended. In such cases the subject increased his muscle activity again in order to re-activate the up state. In a few other cases, such as between roughly 37s and 42s in Fig. 16a, the subject had to brake a flexion motion that was too fast by re-activating the up state. Given the quick increase of M_{hip} following the flexion motion it seems this was an automatic muscle reflex of the hip muscles that may require a further fine-tuning of the controller. In addition it can be seen that especially when lifting heavy loads the maximum M_{hip} and T_{motor} were reached often during lifting up. This limitation will be further relaxed, however, with subsequent experimentation. Overall the lifting assistance provided by the exo-spine was successful in enabling the subject to lift up heavy loads.

As for the ROM of the exo-spine, when comparing it to the human spinal ROM it can be seen that only the flexion ROM is about 10deg less [22]. Although it could be extended by adding a vertebra and a link, it would not be advisable as the human spine becomes weaker when fully flexed [23]. When comparing the maximum ROM of each DOF with the ROM used in the experiment, it can be concluded that while the flexion ROM was used completely, there was still movability left in the other DOF. In the case of rotation (Fig. 15b) about 2/3 of the total ROM was used. Here, the main limitations were the allowable space for the load as well as the torque from the exo-spine pushing the wearer back toward the neutral position, especially with higher loads. Similarly, the assisting torque during lateral flexion was the reason that less than 50% of the lateral flexion ROM was used. With more load on the lower arm this motion actually becomes easier, but further experiments using more active DOF would be needed to confirm whether more motion is actually required. Lastly, shoulder abduction was used mostly in combination with rotation and for about 2/3. However, it will only become really required when the whole trunk flexes forward for deep bending motions.

With the increases in DOF there is, however, also a substantial amount of friction in the system due to the use of rod ends. Although this results in energy losses when lifting something up, it actually

reduces the amount of motor torque when standing still or moving down. Moreover, as can be seen in the experiment results, even when continuously moving up and down the percentage of time the controller spends in the up state is still quite low. With the controller furthermore in the down state when the exo-spine is not moving, it may be concluded that the friction actually helps to save energy.

The exo-spine is, to the authors' knowledge, one of yet very few examples of the application of fDOF into devices that mechanically interact with the human body (one example in [24]). Although its full usefulness will only come into play once the hip motors are added, if successful it could lead to other mechanically optimal solutions for exoskeletons. Examples include more efficient solutions for assisting the fDOF that spans the ankles, knees and hip [15], wrist support combined with elbow actuation into one motor, and actuators that span two or more joints through cables [25] [26], much like some muscles span two joints.

5. CONCLUSIONS

This paper addressed the importance of the current flexibility limitations in full body exoskeletons, particularly for applications in the health care field. A solution called exo-spine was proposed in order to fulfill the purpose of this paper: to enable 3 DOF spinal and 2 DOF shoulder girdle motion with augmentation for lifting in the front. The 5 DOF flexibility of the mechanism was confirmed using ROM measurements as well as experiments in which the exo-spine enabled a subject to lift up weights of up to 40 kg on his lower arms using all DOF of his spine while performing motions similar to those used in nursing techniques. From this experiment we could furthermore confirm the performance of the exo-spine and thus its applicability for full body exoskeletons in health care applications.

The exo-spine will first be extended into a full body HAL robot suit in order to test it fully in a health care setting. At this time extensive experimentation will be needed to cover a large range of possible lifting situations in order to verify the full effectiveness. Eventually, health care workers wearing an exoskeleton will be able to, for example, reach behind a patient while leaning over his bed, while in other fields such as rescue operations wearers will be able to find a proper lifting posture when standing on the ruble. As a result, the addition of the spine and shoulder DOF to exoskeletons in general will increase the amount of available lifting postures, thereby enabling successful lifting actions in a much wider range of challenges.

ACKNOWLEDGEMENTS

This work was supported in part by the Global COE Program on "Cybernics: fusion of human, machine, and information systems", as well as the "Funding Program for World-Leading Innovative R&D on Science and Technology (FIRST Program)," initiated by the Council for Science and Technology Policy (CSTP).

REFERENCES

[1] J.M. Tullar, S. Brewer, B.C. Amick, E. Irvin, Q. Mahood, L.A. Pompeii, A.N. Wang, D. Van Eerd, D. Gimeno, and B. Evanoff, Occupational safety and health interventions to reduce musculoskeletal symptoms in the health care sector. *J. Occup Rehabil.*, Epub (2010)

[2] A. Nelson, and A.S. Baptiste, Evidence-based practices for safe patient handling and movement. *Orthop Nurs.*, 25, pp. 366–79 (2006)

[3] R.E.A. Van Emmerik, M.T. Rosenstein, W.J. McDermott, and J. Hamill, Nonlinear Dynamical Approaches to Human Movement, *Journal of Applied Biomechanics*, vol. 20 (2004)

[4] Y. Sankai, Leading Edge of Cybernics: Robot Suit HAL, *International Joint Conference SICE-ICCAS*, Busan (Korea), pp. 27–28 (2006)

[5] K. Yamamoto, K. Hyodo, M. Ishi and T. Matsuo, Development of power assisting suit for assisting nurse labor, *JSME Int. J., Series C: Mechanical Systems, Machine Elements and Manufacturing*, vol 45, n. 3, pp. 703-711 (2002)

[6] J.C. Perry J. Rosen, and S. Burns, Upper-Limb Powered Exoskeleton Design, *Mechatronics, IEEE/ASME Transactions on*, vol.12, no.4, pp. 408-417 (2007)

[7] C. Hirsh and T. Karloski, Design and implementation of mechanized exoskeletons in the armed forces, *Ninth Annual Freshman Conference*, University of Pittsburgh (2009)

[8] M.S. Liszka, Mechanical Design of a Robotic Arm Exoskeleton for Shoulder Rehabilitation, M.S. thesis, Univ. of Maryland (2006)

[9] S. Toyama, and G. Yamamoto, Development of Wearable-Agri-Robot ~mechanism for agricultural work~, *Proc. IEEE/RSJ International Conference on Intelligent Robots and Systems, 2009,* pp.5801-5806 (2009)

[10] A. Schiele, and F.C.T. Van der Helm, Kinematic design to improve ergonomics in human machine interaction, *IEEE Trans Neural Systems and Rehabilitation Eng*, 14(4), pp. 456-69 (2006)

[11] M. Folgheraiter, B. Bongardt, S. Schmidt, J. De Gea, J. Albiez and F. Kirchner, Design of an Arm Exoskeleton Using a Hybrid Model- and Motion-Capture-Based Technique, *Proc. Interfacing the Human and the Robot Workshop, ICRA* 2009, Kobe, Japan (2009)

[12] S.R. Taal and Y. Sankai, Exoskeletal spine and shoulder girdle for full body exoskeletons with human versatility, *Proc. International Conference on Robotics and Automation 2011*, Shanghai, China (2011)

[13] J. Rosen, J.C. Perry, N. Manning, S. Burns and B. Hannaford, The human arm kinematics and dynamics during daily activities – toward a 7 DOF upper limb powered exoskeleton, *Proc. 12th Intl. Conf. on Advanced Robotics,* ICAR '05, pp. 532-539 (2005)

[14] M.L. Latash, J.P. Scholz and G. Schöner, Toward a new theory of motor synergies, *Motor Control*, vol 11, pp. 275-307 (2007)

[15] J.S. Thomas, D.M. Corcos and Z. Hasan, Kinematic and kinetic constrains on arm, trunk, and leg segments in target-reaching movements, *Journal of Neurophysiology*, vol 93, pp. 352–364 (2005)

[16] I. Mizuuchi, S. Yoshiada, M. Inaba, and H. Inoue. The development and control of a flexible-spine for a human-form robot, *Advanced Robotics*, 17(2), pp. 179–196 (2003)

[17] L. Roos, F. Guenter, A. Guignard, and A.G. Billard, Design of a Biomimetic Spine for the Humanoid Robot Robota, *Proc. Biomedical Robotics and Biomechatronics, 2006. BioRob 2006,* pp.329-334 (2006)

[18] S. Hirose, and H. Yamada, Snake-like robots [Tutorial], *Robotics & Automation Magazine, IEEE* , vol.16, no.1, pp.88-98 (2009)

[19] H. Satoh, T. Kawabata, and Y. Sankai, Bathing care assistance with robot suit HAL, *Proc. IEEE International Conference on Robotics and Biomimetics*, 498-503, Guilin, China (2009)

[20] B. Schibye, et al., Biomechanical analysis of the effect of changing patient-handling technique, *App Ergonom,* 34, pp. 115 – 123 (2003)

[21] M. Shogenji, K. Izumi, A. Seo, and K. Inoue, Biomechanical analysis of the low back load on healthcare workers due to diaper changing, *J. of the Tsuruma Health Science Society*, Vol.31(2), p.p.57~69 (2007)

[22] N. Berryman Reese and W.D. Bandy, Joint Range of Motion and Muscle Length Testing, *Elsevier Health Sciences*, pp. 476-477 (2009)

[23] J.L. Gunning, J.P Callaghan, and S.M. McGill, Spinal posture and prior loading history modulate compressive strength and the type of failure in the spine: a biomechanical study using a porcine cervical spine model, *Clinical Biomechanics*, 16:471– 80 (2001)

[24] D. Campolo, D. Accoto, D. Formica, and E. Guglielmelli, Intrinsic Constraints of Neural Origin: Assessment and Application to Rehabilitation Robotics. *IEEE Trans. on Robotics*, 25:492-501 (2009)

[25] J. Veneman, R. Ekkelenkamp, R. Kruidhof, and F. C. T. van der Helm, A series elastic– and bowden–cable–based actuation system for use as torque actuator in exoskeleton-type robots, *Int. J. of Robotics Research*, vol. 25(3), pp. 261–281 (2006)

[26] A.J. van den Bogert, Exotendons for assistance of human locomotion, *Biomed Eng Online*, 2:17 (2003)

RESEARCH ARTICLE

AMERICAN JOURNAL OF
medical genetics
Neuropsychiatric Genetics

A Loss-of-Function Mutation in the *SLC9A6* Gene Causes X-Linked Mental Retardation Resembling Angelman Syndrome

Yumi Takahashi,[1] Kana Hosoki,[1] Masafumi Matsushita,[2] Makoto Funatsuka,[3] Kayoko Saito,[4] Hiroshi Kanazawa,[2] Yu-ichi Goto,[5] and Shinji Saitoh[1]*

[1]Department of Pediatrics, Hokkaido University Graduate School of Medicine, Sapporo, Japan

[2]Deparrtment of Biological Sciences, Graduate School of Science, Osaka University, Osaka, Japan

[3]Department of Pediatrics, Tokyo Womens' Medical University, Tokyo, Japan

[4]Institute of Medical Genetics, Tokyo Womens' Medical University, Tokyo, Japan

[5]Department of Mental Retardation and Birth Defect Research, National Institute of Neuroscience, National Center of Neurology and Psychiatry, Tokyo, Japan

Received 29 November 2010; Accepted 6 July 2011

SLC9A6 mutations have been reported in families in whom X-linked mental retardation (XMR) mimics Angelman syndrome (AS). However, the relative importance of *SLC9A6* mutations in patients with an AS-like phenotype or XMR has not been fully investigated. Here, the involvement of *SLC9A6* mutations in 22 males initially suspected to have AS but found on genetic testing not to have AS (AS-like cohort), and 104 male patients with XMR (XMR cohort), was investigated. A novel *SLC9A6* mutation (c.441delG, p.S147fs) was identified in one patient in the AS-like cohort, but no mutation was identified in XMR cohort, suggesting mutations in *SLC9A6* are not a major cause of the AS-like phenotype or XMR. The patient with the *SLC9A6* mutation showed the typical AS phenotype, further demonstrating the similarity between patients with AS and those with *SLC9A6* mutations. To clarify the effect of the *SLC9A6* mutation, we performed RT-PCR and Western blot analysis on lymphoblastoid cells from the patient. Expression of the mutated transcript was significantly reduced, but was restored by cycloheximide treatment, indicating the presence of nonsense mediated mRNA decay. Western blot analysis demonstrated absence of the normal NHE6 protein encoded for by *SLC9A6*. Taken together, these findings indicate a loss-of-function mutation in *SLC9A6* caused the phenotype in our patient.

Key words: *SLC9A6*; sodium/hydrogen exchanger 6; Angelman syndrome; X-linked mental retardation; nonsense mediated mRNA decay

How to Cite this Article:
Takahashi Y, Hosoki K, Matsushita M, Funatsuka M, Saito K, Kanazawa H, Goto Y-I, Saitoh S. 2011. A Loss-of-Function Mutation in the *SLC9A6* Gene Causes X-Linked Mental Retardation Resembling Angelman Syndrome.
Am J Med Genet Part B 156:799–807.

INTRODUCTION

SLC9A6 mutations were first reported by Gilfillan et al. [2008] in families exhibiting an X-linked mental retardation (XMR) syndrome mimicking Angelman syndrome (AS). Angelman syndrome is characterized by severe developmental delay with absent or minimal speech, ataxia, easily provoked laughter, epilepsy, and microcephaly. The syndrome is caused by loss-of-function of the *UBE3A* gene which is subject to genomic imprinting. Patients with *SLC9A6* mutations resemble patients with AS, but also demonstrate distinctive clinical features including cerebellar atrophy, slow progression of symptoms, increased glutamate/glutamic acid peak on magnetic resonance spectroscopy (MRS), and lack of characteristic abnormalities seen AS patients examined using electroencephalography (EEG). Following the first report in 2008, in 2010 Schroer et al. reported two other families with AS due to *SLC9A6* mutations, and confirmed the findings of Gilfillan et al.

The *SLC9A6* gene is located on Xq26.3, and encodes the ubiquitously expressed Na^+/H^+ exchanger protein member 6, NHE6. The NHE protein family consists of nine members and includes

Grant sponsor: Ministry of Education, Culture, Sports, Science, and Technology, Japan; Grant number: 21591306.
*Correspondence to:
Shinji Saitoh, Department of Pediatrics, Hokkaido University Graduate School of Medicine, N-15, W-7, Kita-ku, Sapporo 060-8638, Japan.
E-mail: ss11@med.hokudai.ac.jp
Published online 2 August 2011 in Wiley Online Library (wileyonlinelibrary.com).
DOI 10.1002/ajmg.b.31221

NHE1-5 which is found in the plasma membrane, and NHE6-9 which is found in the membranes of intracellular organelles such as mitochondria and endosomes. NHE6 is predominantly present in the early recycling endosome membranes, and is believed to have a role in regulating luminal pH and monovalent cation concentration in intracellular organelles [Brett et al., 2002; Nakamura et al., 2005]. Moreover, Roxrud et al. demonstrated that NHE6 in combination with NHE9 participated in regulation of endosomal pH in HeLa cells by means of the procedure of co-depletion of NHE6 and NHE9 [Roxrud et al. 2009], indicating the significant role of NHE6 in fine-tuning of endosomal pH in human cells. In the brain, exocytosis from recycling endosomes is essential for the growth of dendritic spines which grow during long-term potentiation (LTP). In the absence of recycling endosomal transport, spines are rapidly lost, and LTP stimuli fail to elicit spine growth [Park et al., 2006]. Thus, NHE6 has an important role in the growth of dendritic spines, and also in the development of normal brain wiring. Thus far, five *SLC9A6* mutations have been reported in six AS families; two nonsense mutations, one inframe deletion, one frameshift deletion, and one splicing mutation [Gilfillan et al., 2008; Schroer et al., 2010]. The precise pathogenesis by which these mutations produce disease remains to be clarified.

The aim of this study was to clarify the incidence and importance of *SLC9A6* mutations in AS-like patients and patients with XMR, and to shed light on the molecular pathogenesis of disease due to *SLC9A6* mutations.

MATERIALS AND METHODS

Enrolled Patients

We examined 22 affected Japanese males clinically suspected of having AS but who lacked the genetic abnormalities reported in AS (AS-like cohort). These patients had AS excluded by having negative results for the *SNURF-SNRPN* DNA methylation test (which identifies a deletion, uniparental disomy, or imprinting defect) and *UBE3A* mutation screening (performed as described previously) [Saitoh et al., 2005]. We also examined DNA samples from 104 Japanese patients suspected of having XMR (XMR cohort). The XMR samples were collected as a part of a project for the Japanese Mental Retardation Consortium [Takano et al., 2008]. This study was approved by the Institutional Review Board of Hokkaido University Graduate School of Medicine, and written informed consent was obtained from the parents of the enrolled patients.

Mutation Analysis of the *SLC9A6* Gene

We amplified each exon, including exon–intron boundaries, of the *SLC9A6* gene using polymerase chain reaction (PCR), and all amplicons were directly sequenced on an ABI 3130 DNA analyzer (Applied Biosystems, Foster City, CA) using BigDye Terminator V.1.1 Cycle Sequencing Kit (Applied Biosystems). *SLC9A6* encodes two alternatively spliced transcripts produced from alternative splicing donor sites in exon 2 which give rise to a long form designated as variant 1, and a short form called variant 2. Variant 1 and variant 2 code for NHE6.1 (isoform a) and NHE6.0 (isoform b), respectively (Fig. 1). The primers were designed to amplify each transcript variant. The primers sequence used for amplification and sequencing are available on request. Genomic DNA (10 ng) extracted from peripheral blood was amplified in a total PCR volume of 20 µl containing 1× buffer, 0.4 µM of each primer (forward/reverse), 0.18 mM dNTPs, 0.5 U AmpliTaq Gold® DNA Polymerase (Applied Biosystems). The PCRs for all exons except exon one were performed at 94°C for 10 min followed by 30 cycles of 94°C for 30 sec, 55°C for 30 sec, 72°C for 30 sec, then one cycle at 72°C for 7 min. The high CpG content of exon 1 required it to be amplified in a total reaction volume of 20 µl containing 1× buffer, 0.4 µM of each primer, 0.2 mM dNTPs, 0.4 U Phusion® Hot Start High-Fidelity DNA Polymerase (Finnzymes, Vantaa, Finland), and 3% DMSO. The thermocycling conditions for exon 1 were 98°C for 3 min followed by 35 cycles of 98°C for 10 sec, 65°C for 30 sec and 72°C for 30 sec and then one cycle of 72°C for 5 min. The PCR products were purified with Wizard® PCR Preps DNA Purification System (Promega, Madison, WI) prior to sequencing. All mutations are referred to in relation to reference sequence NM_001042537.

Cell Culture and Cycloheximide Treatment

Epstein–Barr virus (EBV)-transformed lymphoblastoid cells lines were established from peripheral blood cells using standard methods. To prevent potential degradation of transcripts containing premature translation termination codons (PTCs) by nonsense mediated mRNA decay (NMD), lymphoblastoid cells from the patient with the *SLC9A6* mutation and normal controls were treated with 100 µg/ml cycloheximide (CHX) (Sigma, St. Louis, MO). This compound interferes with NMD through inhibition of protein synthesis [Aznarez et al., 2007]. CHX or a 0.1% DMSO control vehicle was used 4 hr prior to RNA extraction from the cell lines [Carter et al., 1995].

RT-PCR

Total RNA from cultured lymphoblastoid cells from the patient and four normal controls, was extracted using the RNAqueous® Kit (Applied Biosystems). Reverse transcription was performed using 100 ng of total RNA and the High-Capacity cDNA Reverse Transcription Kit (Applied Biosystems) in a total reaction volume of 20 µl containing 1× Random primers, 4 mM dNTP mix, 2.5 U of Multiscribe™ Reverse Transcriptase, and 1 µl of RNase Inhibitor. The reactions were incubated at 25°C for 10 min, then at 37°C for 120 min and then followed by 85°C for 5 min to inactivate the reverse transcriptase. Complementary DNA was then amplified using a primer set designed to amplify exon 2–5; forward 5′-GTCTTTTGGTGGGCCTTGT-3′, reverse 5′-GTCCCGTTACC-TTCATCAG-3′. PCR products for NHE6.1 (transcript variant 1) and NHE6.0 (transcript variant 2) were 399 and 303 bp, respectively.

Real-Time Quantification of *SLC9A6* mRNA

To measure *SLC9A6* transcript variant 1 and variant 2, both of which are alternative splicing products, primers and TaqMan® MGB probes were designed with Primer® Express Software (Applied Biosystems; Fig. 1). The Primer and MGB probe sequence

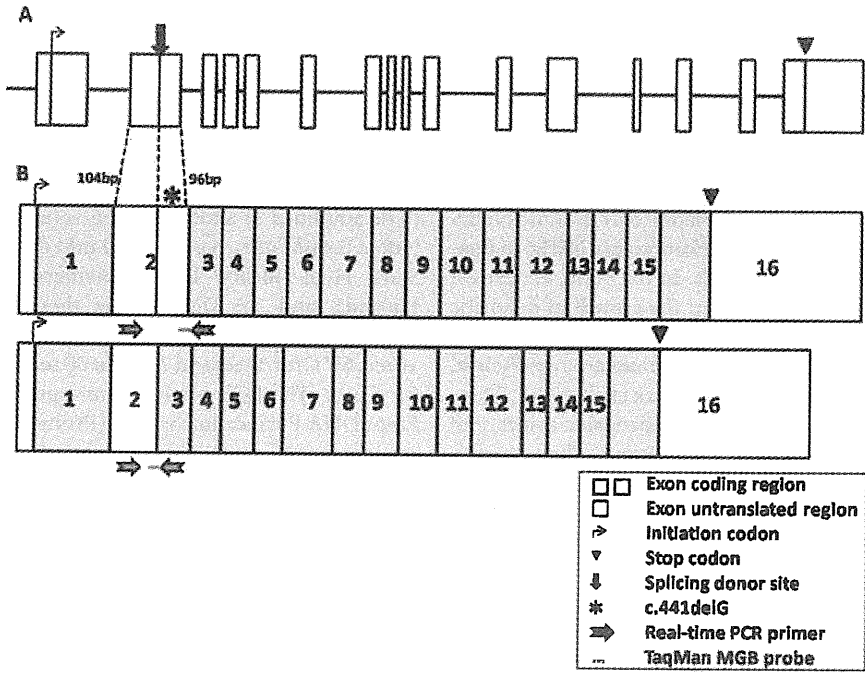

FIG. 1. A: Genomic structure of the *SLC9A6* gene. B: Two alternatively spliced transcripts of the *SLC9A6* gene. Above: *SLC9A6* transcript variant 1 (encodes NHE6.1 or isoform a). Below: *SLC9A6* transcript variant 2 (encodes NHE6.0 or isoform b). The location of the *SLC9A6* mutation in our patient is shown with *. Primers and probes used in real-time quantitative PCR are shown (horizontal arrows).

for variant 1 were forward primer 5′-TGAGTATATGCTGAAAGGAGAGATTAGTTC-3′, reverse primer 5′-GATAGGAGGAAGTAATATGTTGAAAAATACTTC-3′, TaqMan MGB probe 5′-CTTAGAAAGGTTACTTTTGATCC-3′; and for variant 2 forward primer 5′-CTGTGAAGTGCAGTCAAGTCCAA-3′, reverse primer 5′-GATAGGAGGAAGTAATATGTTGAAAAATACTT-3′, TaqMan MGB probe 5′-CTACCTTACTGGTTACTTTTGA-3′. Human *GAPDH* MGB probe and primers purchased from Applied Biosystems were used as the internal control. Patient cDNA was transcribed from 10 ng of total RNA in a total volume of 25 µl containing 1× TaqMan® Universal PCR Master Mix (Applied Biosystems), 0.9 µM of each primer (sense/antisense) and 0.25 µM of probe. Thermocycling was 95°C for 10 min, followed by 40 cycles of 95°C for 15 sec and 60°C for 1 min. Real-time quantitative PCR was performed using the ABI PRISM 7700 (Applied Biosystems). The $2^{-\Delta\Delta Ct}$ method was used for relative quantification.

Western Blot Analysis

HeLa cells and cultured lymphoblastoid cells from the patient, mother and normal controls were washed with phosphate buffered saline and suspended in lysis buffer (phosphate buffered saline containing 1% Triton-X, 1 µg/ml aprotinin, 1 µg/ml pepstatin A, and 1 µg/ml leupeptin). HeLa cells expressing the NHE6.1 were used as a control. The cells were disrupted by sonication and centrifuged at 20,000*g* for 10 min at 4°C. The supernatants were then resolved by SDS-polyacrylamide electrophoresis and transferred to polyvinylidene fluoride membrane (Millipore, Billerica, MA). NHE6 was detected with rabbit polyclonal anti-NHE6 antibody [Ohgaki et al., 2008], anti-rabbit IgG antibody conjugated with horseradish peroxidase (Vector Laboratories, Burlingame, CA) and chemiluminescence reagent (ECL Western Blotting Detection System; GE Healthcare, Waukesha, WI).

RESULTS

Identification of a *SLC9A6* Mutation

We identified only one male patient with a frameshift mutation (c.441delG, p.S147fs) in exon 2, out of 22 male patients in the AS-like cohort (Fig. 2). This frameshift mutation causes a PTC. His healthy mother was heterozygous for the mutation.

No mutation in the *SLC9A6* gene was identified in the XMR cohort. However, two common polymorphisms (rs2291639, rs2307131), and one putative novel polymorphism in intron 12 (c.1692 +10 A>G) were detected.

Clinical Features of the Patient With the *SLC9A6* Mutation

The affected male patient at birth suffered from mild neonatal asphyxia, however he had no other perinatal problems. His parents

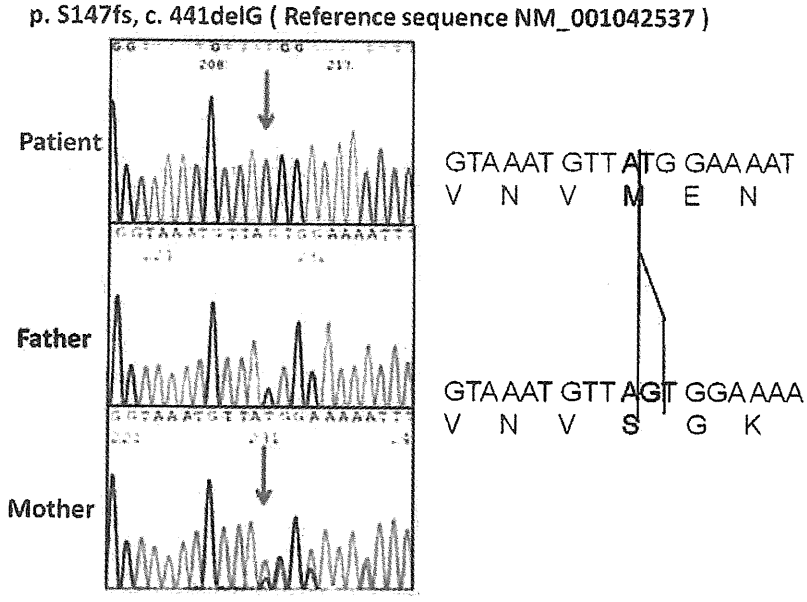

FIG. 2. Chromatographs showing the *SLC9A6* mutation in our patient, and the equivalent genomic region in both his parents. The mutation c.441delG is located in exon 2 and is only present in transcript variant 1. His mother was heterozygous for this mutation, while his father did not have the mutation. This mutant transcript leads to premature protein truncation. The mutation is described relative to reference sequence NM_001043537. [Color figure can be seen in the online version of this article, available at http://onlinelibrary.wiley.com/journal/10.1002/(ISSN)1552-485X]

were non-consanguineous and he did not have any family history of neurological diseases. Although formal clinical assessment was not conducted to the mother, she is healthy and does not have intellectual disability. His clinical features are summarized in Table I. He showed typical findings of AS; severe developmental delay with absence of verbal language, generalized hypotonia, easily provoked laughter, epilepsy, ataxia, strabismus, and microcephaly. His occipitofrontal head circumference at birth was 33.8 cm (+0.4 SD), but his head growth has decelerated into 51.5 cm (−3.0 SD) at 18 years of age. He acquired head control at three months of age, sat and crawled at 6 months of age, and walked unassisted at 18 months of age. His first epileptic attack occurred at 4 years of age. After this first attack, he lost his ability to walk until he was 5 years old. His epileptic attacks consisted of multiple types of seizures, and they were difficult to control with ACTH or several anti-epileptic drugs. TRH treatment improved his awakening and activity levels, and he transiently acquired the ability to walk. However, subsequently his ability to walk was lost, probably due to exacerbation of ataxia. His deep tendon reflex was not increased and no other features of spasticity or peripheral neuropathy were identified. His EEG findings included a background frequency of 5–6 Hz theta waves and spontaneous appearance of 3 Hz diffuse high voltage slow waves. TRH did not change the frequency of his seizures or his EEG findings. He showed no cerebellar atrophy on magnetic resonance imaging (MRI) at 5 years of age. MRS was not performed. He had a normal G-banding karyotype.

Downregulation of the *SLC9A6* Variant 1 in the Patient With the Mutation

The identified mutation c.441delG is located in exon 2 and is only present in variant 1 (Fig. 1). Therefore, the mutation only affects NHE6.1, leaving NHE6.0 intact. Reverse transcriptase PCR demonstrated that *SLC9A6* variant 1 mRNA expression decreased in our patient (Fig. 3A) compared to that in four normal controls. On the other hand, variant 2 expression was increased in the patient compared to the controls. To further investigate mutant *SLC9A6* gene expression, real-time quantitative PCR (qPCR) was performed using cDNA from the patient and normal controls. Quantitative PCR confirmed that *SLC9A6* variant 1 was significantly downregulated in the patient, while it was not downregulated in normal controls (Fig. 4A). Furthermore, the *SLC9A6* variant 2 mRNA in the patient was significantly increased compared to normal controls (Fig. 4B).

Nonsense Mediated Decay Was Involved in the Downregulation of Mutant *SLC9A6* in the Patient

To investigate the possible involvement of NMD in the downregulation of mutant *SLC9A6* in the patient's lymphoblastoid cells, we treated the cells with CHX. After CHX treatment, the expression level of *SLC9A6* variant 1 increased compared to normal control samples on RT-PCR (Fig. 3B). It was also proved that the expression level of variant 1 was significantly increased by performing qPCR, while the expression level in normal control samples

TABLE I. Clinical Findings in Affected Males Previously Reported and Our Patient

Family number: report affected males number (examined number)	1: Gilfillan et al. [2008] 3 (3)	2: Gilfillan et al. [2008] 2 (1)	3: Gilfillan et al. [2008] 3 (3)	4: Gilfillan et al. [2008], Christianson et al. [1999] 16 (4)	5: Schroer et al. [2010] 6 (6)	6: Schroer et al. [2010] 1 (1)	Our patient
Development and behavior							
Profound delay	+	+	+	+	+	+	+
Verbal language absent	+	+	+	+	+	+	+
Easily provoked laughter	+	+	+	+	3/6	−	+
CNS findings							
Epilepsy	+	+	+	+	+	+	+
Ataxia	+	+	+	+	NR	NR	+
Hyperkinetic movements	2/3	−	+	−	2/6	NR	−
Strabismus	+	+	+	+	5/6	+	+
Physical findings							
Microcephaly	+	+	+	3/4	5/6	+	+
Open mouth + drooling	2/3	+	+	NR	4/6	+	+
Swallowing difficulty	2/3	+	1/3	1/4	NR	+	−
Flexed arms	+	NR	1/3	+	3/6	−	−
Electroencephalography							
Epileptiform activity	+	+	+	+	+	+	+
Background activity	10–11 Hz	1.5–3 Hz	4–7 Hz	3–6 Hz to 11–14 Hz	NR	α rhythm	5–6 Hz
Brain MRI/autopsy							
Cerebellar atrophy	1/3	NR	NR	2/4	2/6	+	−
Mutation	p.E287_S288del c.936_941delAAAGTG	p.R500X c.1574C → T	p.V176_201del c.679 +1 delGTAA	p.H203fs c.684_685delAT	p.R500X c.1574C → T	p.Q437X c.1391C → T	p.S147fs c.441delG

+, present with all the patients; −, not present; NR, not recorded.

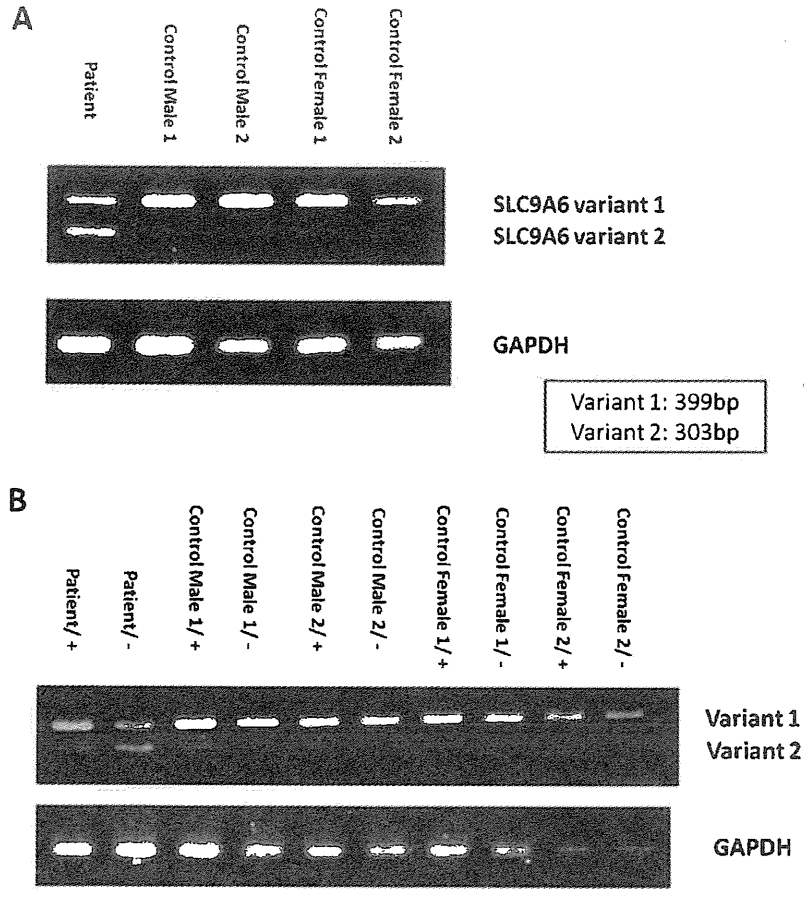

FIG. 3. RT-PCR amplification of the *SLC9A6* gene. A: *SLC9A6* variant 1 mRNA expression was decreased in the patient compared to that in four normal controls. On the other hand, variant 2 expression was increased in the patient compared to that in the controls. B: CHX treatment increases the mutant *SLC9A6* variant 1 mRNA expression, leading to similar expression levels in the patient and four normal controls samples. (+) After CHX treatment, (−) no CHX treatment.

was unchanged (Fig. 4A). The expression level of *SLC9A6* variant 2 increased in all samples after CHX treatment, however the increase was significant only in control samples (Fig. 4B).

Decreased Expression of the NHE6 Protein From Mutant *SLC9A6*

Western blotting was performed to investigate expression of the NHE6 protein in the homogenate of lymphoblastoid cell lines from the patient and his mother. As a result, protein expression of NHE6.1 was not detected in the patient (Fig. 5A,B). The same NHE6.1 was detected in HeLa cells and cells from the patient's mother as well as in the controls. NHE6.0, which was expected to be 10–20 kDa smaller than NHE6.1on SDS–PAGE [Ohgaki et al., 2008], was not detected in any sample (Fig. 5B).

DISCUSSION

In this study we investigated 22 male AS-like patients and 104 male patients with XMR, and identified only one AS-like patient with a *SLC9A6* frameshift mutation. This result further confirms *SLC9A6* is not a major cause of AS-like cases, as reported by Fichou et al. [2009]. Although the number of patients with XMR in this study was small, *SLC9A6* is likely to account for only small proportion of XMR cases.

Patients with *SLC9A6* mutations reported by Gilfillan et al., exhibit cardinal features similar to those of AS including severe developmental delay, mental retardation with absent or minimal use of words, easily provoked laughter, ataxia, epilepsy, hyperkinetic movement, nystagmus, and microcephaly.

Gilfillan et al. also identified possible features of difference between these patients and AS patients, including slow progression of symptoms, thin body, cerebellar atrophy, increased glutamate/

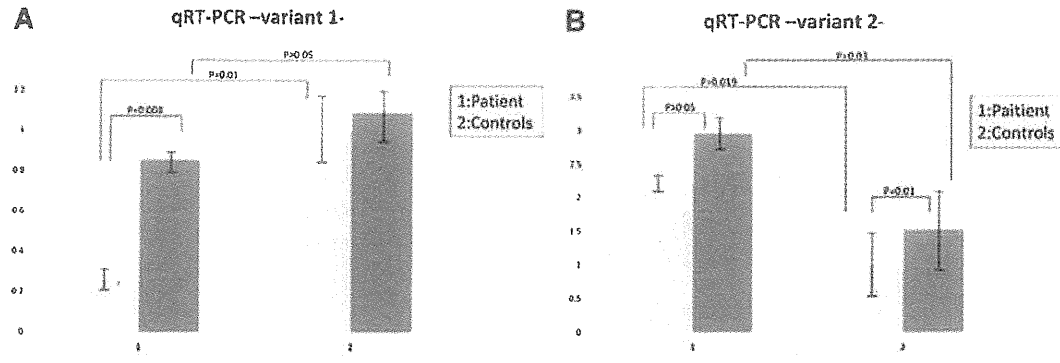

FIG. 4. Real-time quantitative PCR in samples from cell lines from the patient and four normal controls containing two males and two females. The light gray bars indicate the expression levels of *SLC9A6* before CHX treatment, while deep gray bars after CHX treatment. We performed statistical analysis using paired and unpaired Student's *t*-test. Error bars show standard deviation. A: The *SLC9A6* variant 1 was significantly downregulated in samples from the patient while it was not downregulated in samples from four normal controls. After CHX treatment, expression level of the *SLC9A6* variant 1 mRNA in the patient's sample was significantly increased. B: The *SLC9A6* variant 2 in the patient's sample was significantly increased compared to normal controls. Expression level of *SLC9A6* variant 2 increased in all samples after CHX treatment, but a significant increase was only seen in samples from controls.

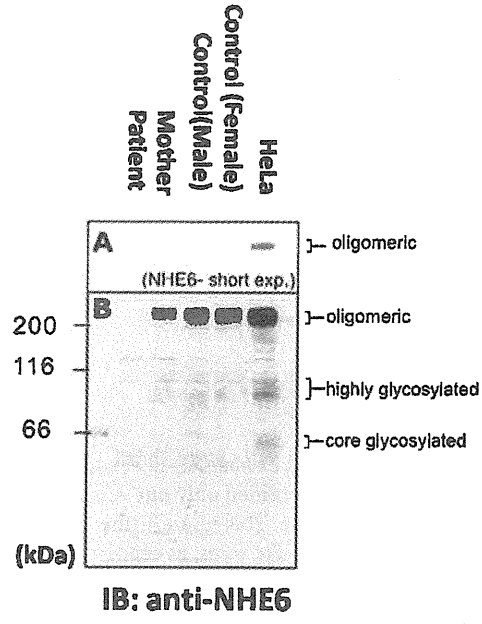

FIG. 5. Protein expression of NHE6 in cultured lymphoblastoid cells and HeLa cells. In the patient, no protein expression of NHE6 isoforms was detected with Western blotting using anti-NHE6 antibody. A: A cropped image taken using a short exposure time demonstrating the oligomeric form of NHE6. Protein size in kDa is shown by numbers on the left of the image. B: A chemiluminescence image of Western blotting taken with a longer exposure time.

glutamic acid peak on MRS, and rapid frequency of 10–14 Hz waves on EEG (Table I). Our patient lost his ability to walk although he did not demonstrate spasticity, demonstrating a slowly progressive clinical course consistent with findings in Gilfillan's report. Indeed, slow progression may be a distinctive clinical feature for patients with *SLC9A6* mutations. One of the families which Gilfillan et al. investigated was previously reported by Christianson et al. [1999], and designated as Christianson syndrome. Schroer et al. reported patients with Christianson syndrome, and they showed that the patients demonstrated an AS-like phenotype. However, while the clinical features of our patient were consistent with those of most patients previously reported by Gilfillan, there were differences including the EEG findings and lack of cerebellar atrophy. Despite this, our patient did meet the diagnostic criteria for AS [Williams et al., 2006]. Therefore, this study further demonstrated that a patient with a *SLC9A6* mutation may resemble patients with AS. Further, this striking similarity between patients with AS and those with *SLC9A6* mutations suggests a possible relationship between the gene function of *UBE3A* and *SLC9A6* in the developing brain.

Our patient's mutation created a frameshift resulting in 7 missense amino acids followed by a stop codon. This mutation was present only in *SLC9A6* transcript variant 1. *SLC9A6* mRNA has two transcript variants caused by alternative splicing in exon 2 (Fig. 1), but the role of each variant has not been clarified. The mutation detected in our patient only affects variant 1 sequence, but the phenotype of the patient was as severe as those in previously reported patients. Therefore, our finding suggests that the NHE6.1 plays an important role in brain function.

Nonsense mediated decay is involved in regulating the expression of alternatively spliced forms containing PTCs [Lareau et al., 2007; Ni et al., 2007]. Since the identified mutation was predicted to result in a PTC, we speculated that NMD could be involved in disease pathogenesis. The result of qRT-PCR showed a significant

decrease in *SLC9A6* variant 1 mRNA expression in the patient sample. This reduction was restored by CHX treatment, while *SLC9A6* variant 1 expression was unaltered by CHX treatment in normal control samples. Expression of *SLC9A6* variant 2 in the patient on the other hand, was significantly increased compared to that in control samples, however it was not influenced by CHX treatment. Therefore, the c.441delG mutation in the patient seems to have modified the alternative splicing pattern, leading to an increase in variant 2 expression. Alternatively, low variant 1 could trigger a regulatory feed back on transcription causing the apparent increase in variant 2 expression. A mutation causing premature protein truncation could alter the splicing pattern and lead to exon skipping, use of alternative splice sites, and intron retention [Hentze and Kulozik, 1999; Mendell and Dietz, 2001]. Our results indicated that the c.441delG mutation caused a PTC altered the splicing pattern, and activated NMD machinery then downregulated *SLC9A6* variant 1 expression.

As protein NHE6.1 was not detected, this indicates an absence of intact NHE6.1. NHE6.0 was also not detected. These findings conclusively indicated that the identified mutation should cause total loss-of-function. Recently, Garbern et al. identified cases with an in-frame deletion of three amino acids, who showed milder dysmorphic features and higher gross motor abilities than those in cases previously reported [Garbern et al., 2010]. Their in-frame deletion should not cause total loss-of-function but create a mildly dysfunctional protein. Therefore, severe phenotypes including severe developmental delay and progressive neurological deterioration may be caused by truncated mutations and less severe phenotypes may be caused by missense or in-frame mutations, and such mild phenotypes are likely missed in patients with mild developmental delay.

Given that the *SLC9A6* variant 2 was upregulated, we speculated that upregulated variant 2 might partially compensate for the absence of NHE6.1. However, we could not establish the upregulation of the NHE6.0 protein, rather it was not detected in the patient's lymphoblastoid cells. NHE6.0 may be unstable compared to NHE6.1. Alternately, NHE6.0 translation may be inhibited. Further investigation is required to definitively answer this question.

NHE6 is found in the membranes of early recycling endosomes and transiently in plasma membranes. Its distribution is regulated by RACK1 [Ohgaki et al., 2008]. Recycling endosomal trafficking is essential for the growth of dendritic spines during LTP in the brain [Park et al., 2006]. The function of the protein product of *UBE3A*, E3 ubiquitin ligase, is also associated with dendritic spine morphology. Mice with a maternal null mutation in *Ube3a* are also reported to have defects in LTP, and manifest motor and behavioral abnormalities [Jiang et al., 1998]. In a recent study, *Ube3a* deficient mice demonstrated dendritic spine dysmorphology [Dindot et al., 2008]. Thus, *UBE3A* and *SLC9A6* could interact in a common pathway involved in dendritic spine development, with a mutation in either leading to an AS-like phenotype.

ACKNOWLEDGMENTS

The authors thank Dr. Tadashi Ariga for critical reading of the manuscript.

REFERENCES

Aznarez I, Zielenski J, Rommens JM, Blencowe BJ, Tsui LC. 2007. Exon skipping through the creation of a putative exonic splicing silencer as a consequence of the cystic fibrosis mutation R533X. J Med Genet 44: 341–346.

Brett CL, Wei Y, Donowitz M, Rao R. 2002. Human Na(+)/H(+) exchanger isoform 6 is found in recycling endosomes of cells, not in mitochondria. Am J Cell Physiol 5:1031–1041.

Carter MS, Doskow J, Morris P, Li S, Nhim RP, Sandstedt S, Wilkinson MF. 1995. A regulatory mechanism that detects premature nonsense codons in T-cell receptor transcripts in vivo is reversed by protein synthesis inhibitors in vitro. J Biol Chem 270:28995–29003.

Christianson AL, Stevenson RE, van der Meyden CH, Pelser J, Theron FW, van Rensburg PL, Chandler M, Schwartz CE. 1999. X linked severe mental retardation, craniofacial dysmorphology, epilepsy, ophthalmoplegia, and cerebellar atrophy in a large South African kindred in localized to Xq24–q27. J Med Genet 36:759–766.

Dindot SV, Antalffy BA, Bhattacharjee MB, Beaudet AL. 2008. The Angelman syndrome ubiquitin ligase localizes to the synapse and nucleus, and maternal deficiency results in abnormal dendritic spine morphology. Hum Mol Genet 17:111–118.

Fichou Y, Bahi-Buisson N, Nectoux J, Chelly J, Heron D, Cuisset L, Bienvenu T. 2009. Mutation in the *SLC9A6* gene is not a frequent cause of sporadic Angelman-like syndrome. Eur J Hum Genet 17:1378–1380.

Garbern JY, Neumann M, Trojanowski JQ, Lee VM, Feldman G, Norris JW, Friez MJ, Schwartz CE, Stevenson R, Sima AA. 2010. A mutation affecting the sodium/proton exchanger, *SLC9A6*, causes mental retardation with tau deposition. Brain 133:1391–1402.

Gilfillan GD, Selmer KK, Roxrud I, Smith R, Kyllerman M, Eiklid K, Kroken M, Mattingsdal M, Egeland T, Stenmark H, Sjoholm H, Server A, Samuelsson L, Christianson A, Tarpey P, Whibley A, Stratton MR, Futreal A, Teague J, Edkins S, Gecz J, Turner G, Raymond FL, Schwartz C, Stevenson RE, Undlien DE, Stromme P. 2008. *SLC9A6* mutations cause X-linked mental retardation, microcephaly, epilepsy, and ataxia, a phenotype mimicking Angelman Syndrome. Am J Hum Genet 82: 1003–1010.

Hentze MW, Kulozik AE. 1999. A perfect message: RNA surveillance and nonsense-mediated decay. Cell 96:307–310.

Jiang YH, Armstrong D, Albrecht U, Atkins CM, Noebels JI, Eichele G, Sweatt JD, Beaudet AL. 1998. Mutation of the Angelman ubiquitin ligase in mice causes increased cytoplasmic p53 and deficits of contextual learning and long-term potentiation. Neuron 21:799–811.

Lareau LF, Inada M, Green RE, Wengrod JC, Brenner SE. 2007. Unproductive splicing of SR genes associated with highly conserved and ultraconserved DNA elements. Nature 446:926–929.

Mendell JT, Dietz HC. 2001. When the message goes awry: Disease-producing mutations that influence mRNA content and performance. Cell 107:411–414.

Nakamura N, Tanaka S, Teko Y, Mitsui K, Kanazawa H. 2005. Four Na^+/H^+ exchanger isoforms are distributed to Golgi and post-Golgi compartments and are involved in organelle pH regulation. J Biol Chem 280:1561–1572.

Ni JZ, Grate L, Donohue JP, Preston C, Nobida N, O'Brien G, Shiue L, Clark TA, Blume JE, Ares M, Jr. 2007. Ultraconserved elements are associated with homeostatic control of splicing regulators by alternative splicing and nonsense-mediated decay. Genes Dev 21:708–718.

Ohgaki R, Fukura N, Matsushita M, Mitsui K, Kanazawa H. 2008. Cell surface levels of organellar Na^+/H^+ exchanger isoform 6 are regulated by interaction with RACK1. J Biol Chem 283:4417–4429.

Park M, Salgado JM, Ostroff L, Helton TD, Robinson CG, Harris KM, Ehlers MD. 2006. Plasticity-induced growth of dendritic spines by exocytic trafficking from recycling endosomes. Neuron 52:817–830.

Roxrud I, Raiborga C, Gilfillan GD, Strømmed P, Stenmark H. 2009. Dual degradation mechanisms ensure disposal of NHE6 mutant protein associated with neurological disease. Exp Cell Res 135:3014–3027.

Saitoh S, Wada T, Okajima M, Takano K, Sudo A, Niikawa N. 2005. Uniparental disomy and imprinting defects in Japanese patients with Angelman syndrome. Brain Dev 27:389–391.

Schroer RJ, Holden KR, Tarpey PS, Matheus MG, Griesemer DA, Friez MJ, Fan JZ, Simensen RJ, Stromme P, Stevenson RE, Stratton MR, Schwartz CE. 2010. Natural history of Christianson syndrome. Am J Med Genet Part A 152A:2775–2783.

Takano K, Nakagawa E, Inoue K, Kamada F, Kure S, Goto Y, Japanese Mental Retardation Consortium. 2008. A loss-of-function mutation in the FTSJ1 gene causes nonsyndromic X-linked mental retardation in a Japanese family. Am J Med Genet Part B 147B:479–484.

Williams CA, Beaudet AL, Clayton-Smith J, Knoll JH, Kyllerman M, Laan LA, Magenis RE, Moncla A, Schinzel AA, Summers JA, Wagstaff J. 2006. Angelman Syndrome 2005: Updated consensus for diagnostic criteria. Am J Med Genet Part A 140A:413–418.

遺伝子診療のなかでの遺伝カウンセリングの基礎と実践

斎藤加代子[*1,2]　浦野真理[*1]　松尾真理[*1]　佐藤裕子[*2]

ゲノム研究の進歩により，診療の現場において確定診断としての遺伝子検査が利用され，発症前診断，保因者診断，出生前診断が可能な時代となった。遺伝子情報は個人と血縁者で共通性があり診断結果が血縁者へ影響を及ぼす場合がある。遺伝子情報漏洩の危険性，遺伝的差別への危惧など倫理的法的社会的問題が生じる可能性もある。このような背景を考えて，遺伝カウンセリング実施体制の構築が必要である。ここでは，遺伝性疾患を例として，遺伝カウンセリングの基礎と実践について述べる。

はじめに

National Society of Genetic Counselors は，2006年に遺伝カウンセリングを次のように定義している[1]。

「人々が遺伝性疾患における医学的，心理学的，家族的影響について理解し，それに適応できるように支援するプロセスである。このプロセスは，以下を統合したものである。

- 疾患の発生または再発の可能性を評価するための家族歴や病歴の解釈
- 遺伝，検査，管理，予防，資源，および研究に関する教育
- リスクまたは状況に対するインフォームドチョイスや適応を促すためのカウンセリング」

遺伝カウンセリングは，遺伝に関する不安に対してメンデル遺伝の法則，経験的再発率，Bayes 分析などにより確率的回答をする時代から，遺伝子検査を行い，同定された遺伝子変異から疾患の確定診断・治療方針の決定を行い，本人および血縁者の発症前診断，保因者診断，出生前診断がなされる時代になってきた。主治医，臨床遺伝の専門家，臨床心理専門職，遺伝看護師，ソーシャルワーカーなどが協力をしてチーム医療を行い，遺伝学に関する正しい知識と情報を共有し，本人・家族への医療，心理，社会的支援を行うことが遺伝カウンセリングである。

1．遺伝子情報の取り扱い

UNESCO の「ヒト遺伝情報に関する国際宣言(2003)」[2]第14条では，「プライバシー及び機密性として，個人を特定できるヒト遺伝情報，ヒトのプロテオーム情報及び生物学的試料は（中略）第三者，特に雇用主，保険会社，教育機関及び家族に対して開示，若しくは入手可能とすべきではない。ヒト遺伝情報，ヒトのプロテ

＊1，2　Saito Kayoko　＊1　東京女子医科大学附属遺伝子医療センター，＊2　東京女子医科大学大学院先端生命医科学系専攻遺伝子医学分野
＊1　Urano Mari，Matsuo Mari
＊2　Sato Yuko

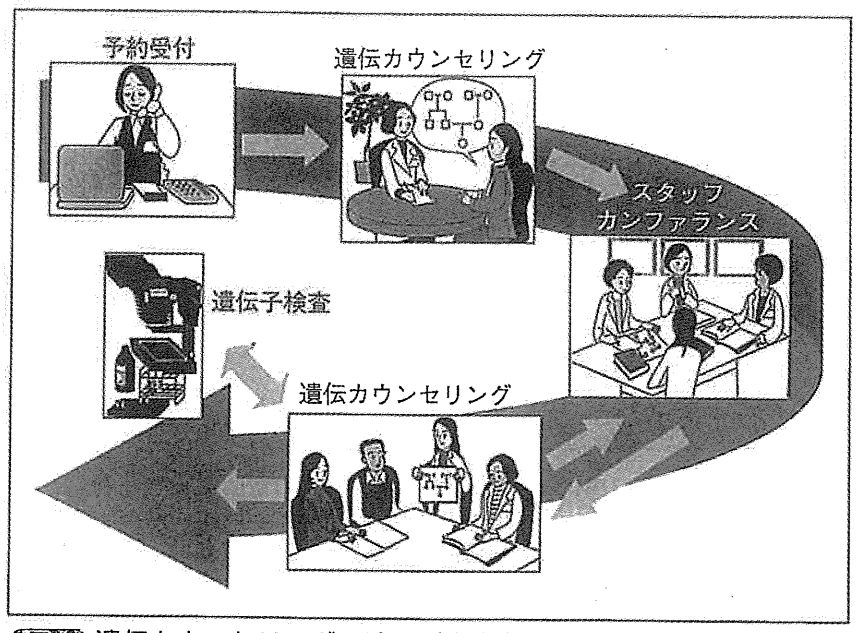

図1 遺伝カウンセリングの流れ（東京女子医科大学遺伝子医療センターの例）

オーム情報及び生物学的試料を使用する研究に参加する個人のプライバシーは保護され，これらの情報は機密情報として取扱われるべきである」と述べられている。厚生労働省「医療・介護関係事業者における個人情報の適切な取扱いのためのガイドライン（2004）」[3]にも「これが漏えいした場合には，本人及び血縁者が被る被害及び苦痛は大きなものとなるおそれがある。したがって，検査結果及び血液等の試料の取扱いについては，UNESCO 国際宣言，医学研究分野の関連指針及び関連団体等が定めるガイドラインを参考とし，特に留意する必要がある。」とされている。一方で，薬理遺伝学的検査（PGx 検査）の臨床現場における普及により，薬剤の副作用の出現予測や薬剤必要量の予測が可能となった。被験者の薬物治療において，遺伝子情報である PGx 検査結果を医師，看護師，薬剤師，臨床検査技師などが共有することで，副作用の出現を防ぎ，適正量を投与するオーダーメイド医療がなされる。遺伝子情報ならば何もかも厳重なセキュリティーのもとに置かなければならないとすると，むしろ弊害が出現することになる。遺伝子情報の内容に合わせた適切なレベルの取り扱いが求められる。

2．遺伝カウンセリングとは

「遺伝カウンセリング」について，UNESCO の「ヒト遺伝情報に関する国際宣言（2003）」[2]第 11 条では「健康に関わる重要な意味を持つ可能性がある遺伝学的検査を行おうとする場合，当事者が遺伝カウンセリングを適切な方法で受けられるようにすべきである。遺伝カウンセリングは非指示的であり，文化的に適合したものであり，かつ当事者の最大の利益と一致したものであるべきである。」と述べている。

遺伝カウンセリング（図 1）では，① 当事者が情報に基づいて決定できるように，個人やカップルに対し，選択肢や医学知識について理解を深めるために援助し，② 当事者がよく理解した上で，その遺伝的問題に対処していくように援助する。また，③ 罪の意識を取り除き，④ 個人やカップルが親となることへの目標を到達できるように援助する。したがって，遺伝カウンセリングにあたる者としては，疾患に対する正しい知識と情報の入手に努めなければならない。近年の分子生物学の進歩によって，遺伝医学はめざましく発展し，疾患の原因遺伝子や原因蛋白質が明らかになってきた。このような進